Temporal convolutional networks for fault diagnosis of photovoltaic systems using satellite and inverter measurements

Jonas Van Gompel
Ghent University - imec
Jonas.VanGompel@UGent.be

Domenico Spina
Ghent University - imec
Domenico.Spina@UGent.be

Chris Develder
Ghent University - imec
Chris.Develder@UGent.be

ABSTRACT

Over time, photovoltaic (PV) systems become increasingly susceptible to faults. Early fault detection and identification not only limits power losses and increases the systems lifetime, but also prevents more serious consequences, such as risk of fire or electrical shock. Although several accurate fault diagnosis methods have been proposed in literature, most PV systems remain unmonitored as the installations are not equipped with the required sensors. In this work, we propose a fault diagnosis technique that does not require on-site sensors. Rather, weather satellite and inverter measurements are used as inputs for the proposed machine learning model. As no dedicated sensors are needed, our method is widely applicable and cost-effective. A temporal convolutional neural network is developed to accurately identify 6 common types of faults, based on the past 24 h of measurements. The proposed approach is tested extensively on a simulated PV system, taking into account multiple severities of each fault type, and reaches an accuracy of over 86%.

CCS CONCEPTS

• **Computing methodologies** → **Supervised learning**; *Neural networks*; • **Hardware** → *Renewable energy*; *Failure prediction.*

KEYWORDS

Fault diagnosis, Photovoltaics, Temporal convolutional network

ACM Reference Format:
Jonas Van Gompel, Domenico Spina, and Chris Develder. 2021. Temporal convolutional networks for fault diagnosis of photovoltaic systems using satellite and inverter measurements. In *The 8th ACM International Conference on Systems for Energy-Efficient Buildings, Cities, and Transportation (BuildSys '21), November 17–18, 2021, Coimbra, Portugal.* ACM, New York, NY, USA, 4 pages. https://doi.org/10.1145/3486611.3486656

1 INTRODUCTION

Reducing the costs and increasing the reliability of solar energy is crucial to expedite the transition to renewable energy. Manufacturing defects and exposure to harsh weather can lead to many types of faults in photovoltaic (PV) systems, such as short circuits or cabling degradation [1]. As preventing all faults in PV systems is generally not possible, accurate and cost-effective fault diagnosis is essential to increase the efficiency and lifetime of PV systems.

This work focuses on fault diagnosis approaches based on machine learning, which avoid the difficulties associated with defining thresholds required for classical approaches [2]. Recently proposed techniques based on machine learning achieve highly accurate fault classification, but rely on the presence of local sensors on the PV system. Commonly required measurements are irradiance and module temperatures [3], output power per module [4], I-V curves [5] and high-frequency current and voltage measurements [6, 7]. However, deploying and maintaining the local sensors required for these measurements is often not feasible for small-scale PV systems. The approach proposed in [8] uses power outputs of nearby PV systems instead of local sensors to detect faults, but cannot identify its type.

Hence, we propose a method that addresses these drawbacks by relying on satellite weather data and inverter measurements of the produced current and voltage at 1 h scale. In contrast to existing methods, which classify faults based solely on the most recent measurement, the proposed methodology takes into account measurements of the past 24 h. Taking the temporal nature of the data into consideration allows for accurate fault diagnosis despite not having access to measurements provided by dedicated on-site sensors. Recently, Bai et al. have shown that temporal convolutional neural networks (TCNs) convincingly outperform popular types of recurrent neural networks for various sequence modelling tasks [9]. Since the proposed methodology formulates the PV fault diagnosis task as a sequence classification problem, a model based on TCNs is developed. The main contributions of our work are:

- A TCN is proposed to accurately detect and identify early manifestations of 6 relevant faults in PV systems.
- By considering 24 h windows of measurements, as opposed to single points in time, the model is able to perform accurate fault diagnosis without relying on local sensors. Instead, the inputs are weather satellite and inverter data. As no installation of sensors is required, the proposed methodology is widely applicable.

2 METHODOLOGY

For a machine learning model to be able to classify faults in a PV system, it must be trained in a supervised setting. This means that the desired output (i.e., no fault, short circuit, etc.) for each input is known during training. As collecting such labelled data experimentally is costly and time-consuming, synthetic training data is generated via physics-based PV simulations, as described in Section 3.1. The newly developed fault diagnosis methodology is summarized in Fig. 1. The input features fed to the model comprise the global horizontal irradiance, ambient temperature, solar zenith angle and the produced current and voltage. The irradiance and temperature are estimated by weather satellite measurements. To

BuildSys '21, November 17–18, 2021, Coimbra, Portugal

ACM ISBN 978-1-4503-9114-6/21/11…$15.00
https://doi.org/10.1145/3486611.3486656

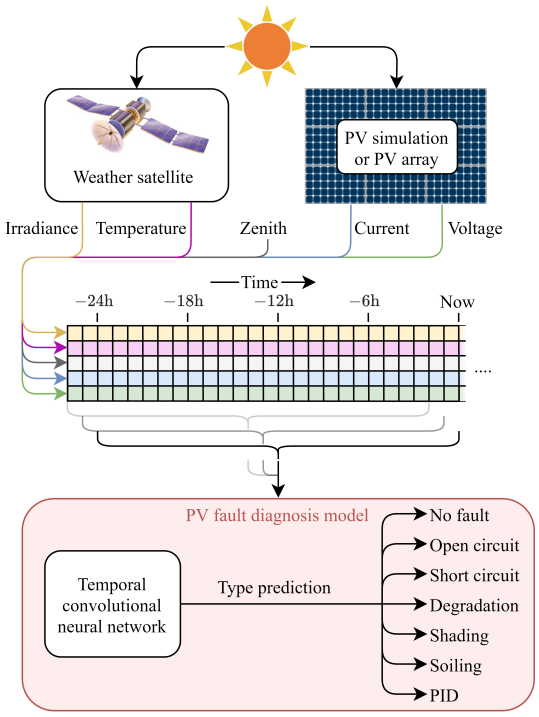

Figure 1: The proposed PV fault diagnosis methodology.

asses the impact of using satellite weather data, which has large error margins, we also compare the performance of the model when using exact weather inputs. From the PV systems' location and time, the zenith of the sun can be easily inferred. During training, the produced current and voltage are estimated via PV simulations. Once implemented, the current and voltage produced by the monitored PV system can be measured by, e.g., the inverter. All 5 input features are recorded with hourly resolution. By sliding over the input features, each 24 h window is classified as either no fault or one of the 6 fault types (see Fig. 1).

3 DATA COLLECTION

3.1 Simulation of faults in PV systems

As gathering sufficient data from PV arrays in the field is infeasible, synthetic training data is generated via cell-level simulations based on the well-established single-diode model [10]. The physics-based PV simulation is adopted from [11]. Realistic weather inputs for the simulations are obtained from sensors at Elizabeth City State University in North Carolina during the period 19 November 2004 – 19 November 2014. These measurements are publicly available in the National Renewable Energy Laboratory (NREL) database [12].

To allow comparison with recently proposed fault diagnosis methods, the PV system under study is the same as in [5, 7]. This PV system is shown in Fig. 2. The specifications of the simulated PV modules are detailed in [13]. The considered faults are also depicted in Fig. 2, while their description is given below:

- The **open circuit** fault is a disconnection in the wiring of the PV system. Two configurations are simulated, namely the disconnection of either 1 or 2 substrings.

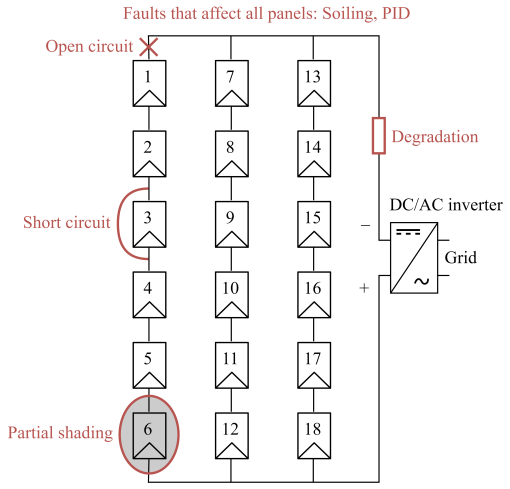

Figure 2: The studied PV system and faults.

- Four severities of **short circuits** are considered: short circuit of module 1, modules 1 and 2, modules 1–3 and lastly modules 1–4.
- Cabling **degradation** leads to an increase of the series resistance of PV modules. Following [5], degradation is simulated by setting the resistance of the resistor in Fig. 2 to 2Ω, 4Ω, 6Ω or 8Ω.
- **Shading** can be cast by clouds or obstacles and is most prominent when the sun is low in the sky. Shading is simulated by reducing the irradiance received by some modules during low sun, defined as the periods with zenith larger than 60°. Four severities of partial shading are considered by reducing the irradiance of:
  - module 18 by 50%,
  - module 18 by 50% and module 17 by 70%,
  - modules 18 and 12 by 50% and module 17 by 70%,
  - modules 18 and 12 by 50% and modules 17 and 11 by 70%.
- **Soiling** occurs when the surface of PV modules is covered by dust or other light absorbing particles. Multiple severities of soiling are considered by reducing the irradiance received by all modules by either 5%, 10%, 15% or 20%.
- The shunting type of **PID**, also known as PID-s, originates from electrochemical degradation caused by a large voltage differences between crystalline silicon PV cells and the frame of the array [1]. This gives rise to a leakage current between the cells and frame. The PID-s simulation is detailed in [14]. Four severities of PID are simulated, corresponding to a 5%, 10%, 15% and 20% loss of average power output.

Overall, 23 configurations of the PV system in Fig. 2 are simulated: no fault, 2 severities of open circuit and 4 severities of all other fault types. We define severity as the average power output reduction caused by the fault. Multiple severities per fault type are considered to ensure the machine learning model does not identify faults by simply recognizing their severity. Each configuration is simulated for 10 years of publicly available weather measurements [12].

3.2 Data preprocessing

Due to missing weather measurements, 12 days of the 10 years were removed. Therefore, the shape of the dataset is $(3640, 23, 24, 5)$, corresponding to the number of days, configurations, hours in a day

and input features, respectively. To minimize the technique's implementation cost, the produced current and voltage will be measured by the inverter instead of dedicated sensors. As inverters can cause relative measurement errors of up to 5%, we will include 5% noise in the current and voltage values obtained from the simulations. To this end, the current I and voltage V vectors are adjusted as $I' = (1 + U_1)I$ and $V' = (1 + U_2)V$, where U_1 and U_2 are noise vectors with elements drawn uniformly from the interval $[-0.05, 0.05]$.

In order to obtain a representative view of the performance of the model, 5-fold cross-validation is performed. First, the order of all days in the dataset is randomly shuffled. Subsequently, the data is divided into 5 subsets of equal size, of which 4 are used to train the model. The remaining subset is further split into validation and test data. The validation data is used for hyperparameter tuning and early stopping (see Section 4.1), while the test data is used to evaluate the model after training. In each of the 5 cross-validation iterations, a different subset is chosen as non-training data.

The data is normalized to prevent numerical instability during training. In particular, normalization of input feature i is performed by determining the mean $\mu_{i,\text{ok}}$ and standard deviation $\sigma_{i,\text{ok}}$ for the configuration without faults in the training data. Each measurement m of input feature i is normalized using

$$m' = \frac{m - \mu_{i,\text{ok}}}{\sigma_{i,\text{ok}}}.$$

Hence only the input features of the configuration without faults will have mean 0 and standard deviation 1. Each configuration is rescaled using the mean and standard deviation of the configuration without faults because the relative scale of the current and voltage between the different configurations is essential information. Both the validation and test data are also normalized using $\mu_{i,\text{ok}}$ and $\sigma_{i,\text{ok}}$, which are obtained from the training data.

By sliding a 24 h window over the input data, the model is able to predict the type of a potential fault each hour, based on the 24 most recent measurements (see Fig. 1). Additionally, the sliding window approach effectively increases the number of training samples, without acquiring new data (i.e., data augmentation). Note that the window does not slide over different configurations, meaning samples with values from two different configurations are not included in the data.

4 MODEL DESCRIPTION

4.1 Temporal convolutional neural network

In this work, the fault diagnosis task is formulated as sequence classification. Since TCNs have been shown to outperform common types of recurrent neural networks [9], they are a natural choice as model architecture. Therefore, we use temporal convolutional (TC) layers to automatically extract features from the input data, after which softmax classification is performed. The model is depicted in Fig. 3. The implementation of [15] was used for the TC layers. Temporal convolutions, also known as causal convolutions, do not include future time steps in the convolution operations. For example, a regular 1D convolution with kernel size 3 would calculate its output at timestep t from inputs at $t-1$, t and $t+1$, while a temporal convolution uses the inputs at $t-2$, $t-1$ and t. This avoids leakage from the future into the past [9].

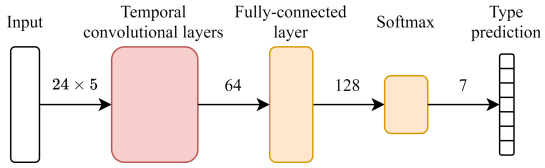

Figure 3: The proposed neural network. The numbers indicate the dimension of the feature vectors that are passed.

In our model, the input data is first processed by 4 TC residual blocks with kernel size 2. As recommended in [9], the dilation of the block at depth d is 2^d, resulting in dilations 1, 2, 4 and 8, respectively. Each block consists of 2 dilated TC layers with the same kernel size and dilation, as described in [9]. After each dilated TC layer, batch normalisation, ReLU and 5% dropout is applied. The last timestep of the output of the final TC residual block is then processed by a fully-connected layer with 128 nodes and 20% dropout, followed by ReLU. Finally, the softmax activation is applied to the output layer which classifies the type of the sample. The values of the hyperparameters described above were manually tuned.

The model is trained by minimizing the cross-entropy loss. The loss is weighed to compensate for the class imbalance in the data: as described in Section 3.1, there is 1 configuration without faults, 2 with open circuit faults and 4 of all other faults. The model is trained with the Adam optimizer and batch size 128. The learning rate $\gamma(\tau)$ at optimization step τ is gradually decreased during training:

$$\gamma(\tau) = \frac{\gamma_0}{1 + \lambda\tau} = \frac{5 \cdot 10^{-3}}{1 + 5 \cdot 10^{-5}\,\tau}.$$

As additional regularization, early stopping is performed, restoring the model to the training epoch at which the highest balanced accuracy on the validation data was reached. The accuracy is balanced to compensate for the class imbalance, analogous to the loss function.

4.2 Reference model: CatBoost

To assess the performance of our proposed model, we compare it against a baseline model, namely CatBoost. CatBoost is a state-of-the-art gradient boosting algorithm which uses ordered boosting to prevent overfitting [16]. The model is trained by minimizing the weighed cross-entropy loss defined in Section 4.1. Note that CatBoost does not take the time dimension of the input into account, so each input sample is first flattened from shape $(24, 5)$ to (120). To prevent overfitting, early stopping is used and the *random_strength* hyperparameter is set to 100. This value was determined via a grid search. For all other hyperparameters, the default values of the implementation in [16] performed best.

5 RESULTS AND DISCUSSION

5.1 Exact weather data

In the first application scenario, accurate on-site weather sensors would be available, which means the model receives the same irradiance and temperature inputs as the PV simulation. The current and voltage produced by the PV system would still be measured by the inverter, so 5% uniform noise is included for these input features (see Section 3.2). In this setting, the TCN reaches 96.8% ± 1.1% balanced accuracy, which is the average and 3 times the standard

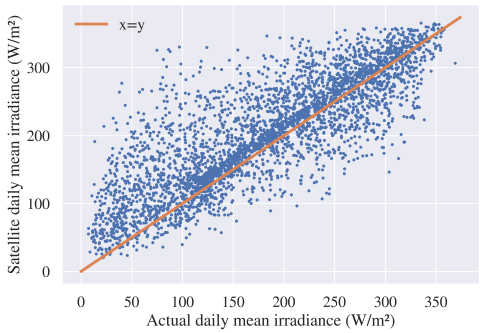

Figure 4: Comparison between the irradiance measured by the on-site sensors and weather satellite estimates.

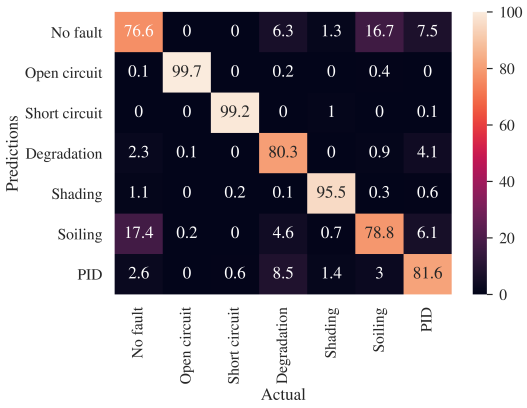

Figure 5: Confusion matrix using satellite weather input. For each fault, the accuracy of all severities are averaged.

deviation over the test sets of the 5-fold cross-validation. Given that the input noise is of similar magnitude as the average power output reduction caused by some of the faults, the achieved accuracy is remarkable. Although CatBoost converges after training for a similar amount of time as the TCN, its performance is inferior: CatBoost reaches 93.2% ± 1.3% balanced accuracy.

5.2 Satellite weather data

In the second scenario, the technique's ability to operate without installed sensors is explored by using satellite derived irradiance and temperature inputs for the model. The used MERRA-2 satellite weather data for North Carolina is publicly available [17]. The irradiance measurements by the on-site sensor and the weather satellite are compared in Fig. 4, where each blue dot represents the mean irradiance of a single day. Note that the weather satellite overestimates the average irradiance by 250 W/m^2 some days. Performing PV fault diagnosis with such inaccurate irradiance input is significantly more challenging than the scenario in Section 5.1, since both a fault and an overestimation of the irradiance will result in observing a lower power output than expected. Nevertheless, the TCN achieves a balanced accuracy of 86.4% ± 1.9%. In Fig. 5, the confusion matrix of the first cross-validation iteration is presented. This figure reveals that substantially more mistakes are made when distinguishing between no fault and soiling, as compared to other classes. This is due to the irradiance overestimations by the satellite, which have a similar effect as soiling: in both cases, the irradiance input of the TCN is higher than what the modules are exposed to in reality. Using satellite weather data, the TCN again outperforms CatBoost, which reaches 83.5% ± 2.1% balanced accuracy.

6 CONCLUSIONS

A methodology is proposed where a temporal convolutional neural network identifies 6 common faults in PV systems, based on a 24 h window of measurements. By taking into account the temporal nature of the data, accurate fault diagnosis is possible without requiring I-V curve tracers, high-frequency measurements or weather sensors, unlike state-of-the-art fault diagnosis methods. Instead, the neural network relies on weather satellite and inverter measurements with low temporal resolution (1 h). As implementing the proposed technique does not require local sensors, it is both cost-effective and broadly applicable.

REFERENCES

[1] M. Koentges, S. Kurtz, C. Packard, U. Jahn, K. A. Berger, K. Kato, *et al.*, *Review of failures of photovoltaic modules*. IEA International Energy Agency, 2014.

[2] D. S. Pillai and N. Rajasekar, "A comprehensive review on protection challenges and fault diagnosis in PV systems," *Renewable and Sustainable Energy Reviews*, vol. 91, pp. 18–40, 2018.

[3] W. Chine, A. Mellit, V. Lughi, A. Malek, G. Sulligoi, and A. M. Pavan, "A novel fault diagnosis technique for photovoltaic systems based on artificial neural networks," *Renewable Energy*, vol. 90, pp. 501–512, 2016.

[4] M. Feng, N. Bashir, P. Shenoy, D. Irwin, and D. Kosanovic, "Sundown: Model-driven per-panel solar anomaly detection for residential arrays," in *Proceedings of the 3rd ACM SIGCAS Conference on Computing and Sustainable Societies*, 2020.

[5] Z. Chen, L. Wu, S. Cheng, P. Lin, Y. Wu, and W. Lin, "Intelligent fault diagnosis of photovoltaic arrays based on optimized kernel extreme learning machine and IV characteristics," *Applied Energy*, vol. 204, pp. 912–931, 2017.

[6] W. Gao, R.-J. Wai, and S.-Q. Chen, "Novel PV fault diagnoses via SAE and improved multi-grained cascade forest with string voltage and currents measures," *IEEE Access*, vol. 8, pp. 133144–133160, 2020.

[7] Z. Chen, F. Han, L. Wu, J. Yu, S. Cheng, P. Lin, *et al.*, "Random forest based intelligent fault diagnosis for PV arrays using array voltage and string currents," *Energy conversion and management*, vol. 178, pp. 250–264, 2018.

[8] S. Iyengar, S. Lee, D. Sheldon, and P. Shenoy, "Solarclique: Detecting anomalies in residential solar arrays," in *Proceedings of the 1st ACM SIGCAS Conference on Computing and Sustainable Societies*, pp. 1–10, 2018.

[9] S. Bai, J. Z. Kolter, and V. Koltun, "An empirical evaluation of generic convolutional and recurrent networks for sequence modeling," *arXiv preprint arXiv:1803.01271*, 2018.

[10] N. Pearsall, *The performance of photovoltaic (PV) systems: modelling, measurement and assessment*. Woodhead Publishing, 2016.

[11] I. Horvath, H. Goverde, P. Manganiello, A. Schils, A. van der Heide, J. Govaerts, *et al.*, "Next generation tools for accurate energy yield estimation of bifacial PV systems – best practices, improvements and challenges," in *EU PVSEC*, 2019.

[12] A. Andreas and T. Stoffel, "Elizabeth City State University: Elizabeth City, North Carolina (data)." NREL Report No. DA-5500-56517, 1985. http://dx.doi.org/10.5439/1052558.

[13] SolarWorld, *SolarWorld Sunmodule Bisun 325 XL duo solar panel data sheet*, 2016. https://d3g1qce46u5dao.cloudfront.net/data_sheet/sunmodule_bisun_xl_solar_panel_325_datasheet.pdf.

[14] A. Schils, J. Carolus, J. Ascencio-Vásquez, A. Wabbes, E. Bertrand, M. Daenen, *et al.*, "A grey box model for shunting-type potential induced degradation in silicon photovoltaic cells under environmental stress," to be published in *EU PVSEC 2021*.

[15] P. Remy, "Temporal convolutional networks for keras." https://github.com/philipperemy/keras-tcn, 2020.

[16] L. Prokhorenkova, G. Gusev, A. Vorobev, A. V. Dorogush, and A. Gulin, "Catboost: unbiased boosting with categorical features," in *Advances in Neural Information Processing Systems*, vol. 31, Curran Associates, Inc., 2018.

[17] R. Gelaro, W. McCarty, M. J. Suárez, R. Todling, A. Molod, L. Takacs, *et al.*, "The modern-era retrospective analysis for research and applications, version 2 (MERRA-2)," *Journal of climate*, vol. 30, no. 14, pp. 5419–5454, 2017. https://www.renewables.ninja/.